

## PROBING GRAVITY AT LARGE SCALES THROUGH CMB LENSING

ANTHONY R. PULLEN, SHADAB ALAM, AND SHIRLEY HO

Department of Physics, Carnegie Mellon University, 5000 Forbes Ave, Pittsburgh, PA, 15213, U.S.A.

*Draft version March 1, 2024*

## ABSTRACT

We describe a methodology to probe gravity with the cosmic microwave background (CMB) lensing convergence  $\kappa$ , specifically by measuring  $E_G$ , the ratio of the Laplacian of the gravitational scalar potential difference with the velocity divergence. Using CMB lensing instead of galaxy-galaxy lensing avoids intrinsic alignments while also lacking a hard limit on the lens redshift and significant uncertainties in the source plane. We model  $E_G$  for general relativity and modified gravity, finding that  $E_G$  for  $f(R)$  gravity should be scale-dependent due to the scale-dependence of the growth rate  $f$ . Next, we construct an estimator for  $E_G$  in terms of the galaxy-CMB lensing and galaxy clustering angular power spectra, along with the RSD parameter  $\beta$ . We also forecast statistical errors for  $E_G$  from the current *Planck* CMB lensing map and the spectroscopic galaxy and quasar samples from the Sloan Digital Sky Survey Data Release 11, being 9% with galaxies and 8% when quasars are included. We also find that upcoming spectroscopic and photometric surveys, combined with the final *Planck* lensing map, can measure precisely the redshift- and scale-dependence of  $E_G$  out to redshifts  $z = 2$  and higher, with photometric surveys having an advantage due to their high number densities. Advanced ACTPol's lensing map will increase the  $E_G$  sensitivity even further. Finally, we find that Advanced ACTPol cross-correlated with spectroscopic (photometric) surveys can differentiate between general relativity and  $f(R)$  gravity at the level of  $3\sigma$  ( $13\sigma$ ). Performing a  $< 1\%$  measurement of  $E_G$  requires a 10% precision in  $\beta$  from *Euclid* or LSST, currently achievable with a spectroscopic survey but difficult with only a photometric survey.

**Keywords:** cosmology: theory, cosmology: observations, gravitation, gravitational lensing: weak, large scale structure of the universe

## 1. INTRODUCTION

The discovery of cosmic acceleration (Riess et al. 1998; Perlmutter et al. 1999) has inspired numerous theoretical explanations for its existence. On one hand, the acceleration can be caused by a new, unknown force that exhibits negative pressure called *dark energy* (Peebles & Ratra 2003). The cosmological constant, a special case of dark energy, is a major component of the  $\Lambda$ CDM framework that explains the expansion history and the growth history of the Universe (Anderson et al. 2014) and the cosmic microwave background (CMB) (Bennett et al. 2013; Planck Collaboration et al. 2013). On the other hand, it is possible that the dynamics of gravity deviate from general relativity (GR) on cosmological scales (Dvali et al. 2000; Carroll et al. 2004), a concept called *modified gravity*. In observations of the universe's expansion history, these two effects are degenerate with one another. However, we expect the growth of structure to differ between dark energy and modified gravity models such that the degeneracy is broken.

An observable that probes the expansion history and growth of structure simultaneously is  $E_G$  (Zhang et al. 2007), which is related to the ratio of the Laplacian of the difference between the two scalar potentials  $\nabla^2(\psi - \phi)$  to the peculiar velocity perturbation field  $\theta$ . The value of  $E_G$  depends on how gravity behaves on large scales. Traditionally, when measuring  $E_G$ ,  $\nabla^2(\psi - \phi)$  is probed by a galaxy lensing correlation with a tracer of large-scale structure (LSS), while the peculiar velocity field is probed by either a galaxy-velocity cross-correlation or,

equivalently, a galaxy autocorrelation times the redshift-space distortion (RSD) parameter  $\beta = f/b$ , where  $f$  is the growth rate and  $b$  is the clustering bias of the galaxies. A major advantage of  $E_G$  over other observables is that it is independent of clustering bias on linear scales, reducing the model uncertainty.  $E_G$  was first measured in Reyes et al. (2010), using galaxy-galaxy lensing exhibited by Sloan Digital Sky Survey (SDSS) (York et al. 2000) Luminous Red Galaxies (LRGs) (Eisenstein et al. 2001) to find  $E_G(z = 0.32) = 0.392 \pm 0.065$ , consistent with  $\Lambda$ CDM.

In this analysis we assess the possibility of using CMB lensing (Blanchard & Schneider 1987; Linder 1988; Cole & Efstathiou 1989) cross correlated with galaxies (Hirata et al. 2004; Smith et al. 2007; Hirata et al. 2008; Planck Collaboration et al. 2014) as a probe of  $\nabla^2(\psi - \phi)$  instead of the traditional method of using galaxy lensing. One advantage of using CMB lensing over galaxy lensing is that the CMB lensing kernel is very broad over redshift, allowing probes of  $E_G$  at much higher redshifts than with galaxy lensing. At these higher redshifts, CMB lensing also has the added bonus of probing more linear scales, reducing systematic effects due to nonlinear clustering. Also, since the CMB propagates throughout all of space, all of LSS sampled by the survey lenses the CMB, allowing us to measure the lensing part of  $E_G$  at much higher redshifts. We also do not have to worry about complex astrophysical uncertainties of the source galaxies, *i.e.* intrinsic alignments, since the CMB is simple. Finally, we know the CMB redshift, so we can avoid determining the photometric redshift distribution of the sources. We construct an estimator for  $E_G$  in terms of the angular

cross-power spectrum between the CMB lensing convergence  $\kappa$  and galaxies, the angular auto-power spectrum of the same galaxies, and the RSD parameter  $\beta$ .

Next, we derive  $E_G$  for general relativity (GR), as well as modified gravity using the  $\mu\gamma$  formalism from Hojjati et al. (2011). While  $E_G(z)$  can be written as  $\Omega_{m,0}/f(z)$  for  $\Lambda$ CDM, where  $\Omega_{m,0}$  is the matter density today relative to the critical density and  $f(z)$  is the growth rate at redshift  $z$ ,  $E_G$  for modified gravity models is expected to differ from this value. We also found that  $E_G$  for  $f(R)$  gravity (Carroll et al. 2004) and chameleon gravity (Khouri & Weltman 2004) can exhibit scale-dependence through  $f$ , which could potentially help differentiate between these gravity models and GR.

Next, we consider the prospect of measuring  $E_G$  with CMB lensing by forecasting errors for an  $E_G$  measurement using the current *Planck* CMB lensing map (Planck Collaboration et al. 2014) along with the CMASS galaxy ( $z = 0.57$ ), LOWZ galaxy ( $z = 0.32$ ), and BOSS quasar (Pâris et al. 2014) spectroscopic samples from Data Release 11 (DR11) (Anderson et al. 2014) of the SDSS-III (Eisenstein et al. 2011) Baryon Oscillations Spectroscopic Survey (BOSS) (Dawson et al. 2013). We also consider possibilities with upcoming surveys. First, we consider the final *Planck* lensing map cross-correlated with spectroscopic surveys, specifically the Dark Energy Spectroscopic Instrument (DESI) (Levi et al. 2013), *Euclid* (Laureijs et al. 2011), and the Wide Field InfraRed Survey Telescope (WFIRST) (Spergel et al. 2013). We find, however, that an  $E_G$  measurement using the *Planck* CMB lensing map and upcoming spectroscopic surveys is not sensitive enough to differentiate between GR and  $f(R)$  gravity at current limits, and that the new limits on chameleon gravity would be modest. We find that spectroscopic surveys with Advanced ACTPol can differentiate between GR and  $f(R)$  gravity at the level of  $3\sigma$ , with higher significances for the chameleon gravity model.

We also consider the CMB lensing maps cross-correlated with photometric surveys, specifically the Dark Energy Survey (DES) (The Dark Energy Survey Collaboration 2005), the Large Synoptic Survey Telescope (LSST) (LSST Science Collaboration et al. 2009), and *Euclid*. We find that for the scales which  $E_G$  dominates, being small but still only quasi-linear, the lensing measurement dominates the error in  $E_G$  as opposed to the RSD. Thus, reducing the shot noise by increasing the survey number density is more important than having more precise redshifts for RSD. We find DES is comparable in power to DESI, and LSST and photometric *Euclid* can discriminate between GR and  $f(R)$  gravity at very high significance using lensing from Adv. ACTPol. However, this will require an RSD precision on the order of 10%, which is difficult but possible for *Euclid* and LSST. Photometric surveys combined with CMB lensing experiments can produce significant constraints to  $E_G$  that could help uncover the true nature of gravity.

The plan of the paper is as follows: in Section 2, we write the theoretical  $E_G$  for modified gravity, while Section 3 gives the estimator for  $E_G$  in terms of CMB lensing. In Section 4 we construct forecasts for various experiment configurations, and in Section 5 we present conclusions. We assume the combined CMASS/*Planck* cosmology (Planck Collaboration et al. 2013; Anderson et al.

2014) with  $\Omega_m h^2 = 0.1418$ ,  $h = 0.676$ ,  $\Omega_b h^2 = 0.0224$ ,  $n_s = 0.96$ , and  $\sigma_8 = 0.8$ .

## 2. THEORY

We begin with the definition of  $E_G$  in Fourier space from Zhang et al. (2007), given by

$$E_G(k, z) = \frac{c^2 [\nabla^2(\psi - \phi)]_k}{3H_0^2(1+z)\theta(k)} = \frac{c^2 k^2(\phi - \psi)}{3H_0^2(1+z)\theta(k)}, \quad (1)$$

where  $H_0$  is the Hubble parameter today and  $\theta(k)$  is the perturbation in the matter velocity field. Assuming a flat universe described by a Friedmann-Robertson-Walker (FRW) metric with perturbation fields  $\psi$  in the time component and  $\phi$  in the spatial component, as well as negligible anisotropic stress and non-relativistic matter species, the time-time and momentum Einstein field equations in general relativity (GR) can be written in Fourier space as (Hojjati et al. 2011)

$$k^2\psi = -4\pi G a^2 \rho(a)\delta \\ \phi = -\psi, \quad (2)$$

where  $a$  is the scale factor,  $\rho$  is the background matter density, and  $\delta$  is the matter density perturbation. These equations are generalized to a modified gravity (MG) model such that

$$k^2\psi = -4\pi G a^2 \mu(k, a)\rho(a)\delta \\ \phi = -\gamma(k, a)\psi, \quad (3)$$

where  $\mu(k, a)$  and  $\gamma(k, a)$  are arbitrary functions of  $k$  and  $a$ , and  $\mu = \gamma = 1$  for GR.

Using this formalism, we can write the numerator of  $E_G$  in Eq. 1 as

$$k^2(\phi - \psi) = -k^2[1 + \gamma(k, a)]\psi \\ = 4\pi G a^2 \rho(a)\mu(k, a)[1 + \gamma(k, a)]\delta. \quad (4)$$

Substituting  $\rho(a) = \rho_0 a^{-3}$  and  $\Omega_{m,0} = 8\pi G \rho_0 / 3H_0^2$ , we find

$$k^2(\phi - \psi) = \frac{3}{2} H_0^2 \Omega_{m,0} (1+z) \mu(k, a) [\gamma(k, a) + 1] \delta \quad (5)$$

The velocity perturbation  $\theta$  can be written as  $\theta = f\delta$  on linear scales. Combining this expression and Eq. 5 gives  $E_G$  from Eq. 1 as

$$E_G(k, z) = \frac{\Omega_{m,0} \mu(k, a) [\gamma(k, a) + 1]}{2f}. \quad (6)$$

This expression gives us the correct value in the GR limit, namely  $E_G = \Omega_{m,0}/f(z)$ .

For  $f(R)$  gravity (Carroll et al. 2004) using the parametrization in Song et al. (2007),  $\mu$  and  $\gamma$  are given by (Tsujikawa 2007; Hojjati et al. 2011)

$$\mu^{\text{fR}}(k, a) = \frac{1}{1 - B_0 a^{s-1}/6} \left[ \frac{1 + (2/3)B_0 \bar{k}^2 a^s}{1 + (1/2)B_0 \bar{k}^2 a^s} \right] \\ \gamma^{\text{fR}}(k, a) = \frac{1 + (1/3)B_0 \bar{k}^2 a^s}{1 + (2/3)B_0 \bar{k}^2 a^s}, \quad (7)$$

where  $\bar{k} = k[2997.9 \text{ Mpc}/h]$ ,  $h = H_0/[100 \text{ km/s/Mpc}]$ ,  $s=4$  for models that follow the  $\Lambda\text{CDM}$  expansion history, and  $B_0$  is a free parameter which is related to the Compton wavelength of an extra scalar degree of freedom and is proportional to the curvature of  $f(R)$  today. Current measurements limit  $B_0 < 5.6 \times 10^{-5}$  ( $1\sigma$ ) (Xu 2014; Bel et al. 2014). For this gravity model,  $E_G$  is given by

$$E_G^{\text{BZ}}(k, z) = \frac{1}{1 - B_0 a^{s-1}/6} \frac{\Omega_{m,0}}{f^{\text{BZ}}(k, z)}, \quad (8)$$

where  $f^{\text{BZ}}(k, z)$  is the BZ growth rate, which is scale-dependent since  $\mu$  is scale-dependent (Hojjati et al. 2011).

Chameleon gravity (Khouri & Weltman 2004) is a Yukawa-type dark matter interaction equivalent to a class of scalar-tensor theories with a scalar field non-minimally coupled to the metric. For chameleon gravity, using the Bertschinger and Zukin (BZ) parametrization (Bertschinger & Zukin 2008),  $\mu$  and  $\gamma$  are given by (Hojjati et al. 2011)

$$\begin{aligned} \mu^{\text{Ch}}(k, a) &= \frac{1 + \beta_1 \lambda_1^2 k^2 a^s}{1 + \lambda_1^2 k^2 a^s} \\ \gamma^{\text{Ch}}(k, a) &= \frac{1 + \beta_2 \lambda_2^2 k^2 a^s}{1 + \lambda_2^2 k^2 a^s} \\ \lambda_2^2 &= \beta_1 \lambda_1^2 \\ \beta_2 &= \frac{2}{\beta_1} - 1, \end{aligned} \quad (9)$$

where the typical ranges for  $\beta_1$  and  $s$  are  $0 < \beta_1 < 2$  and  $1 \leq s \leq 4$ . We will relate  $\lambda_1$  to  $B_0$ , a parameter similar to that for  $f(R)$  gravity but much less constrained due to the extra degree of freedom in the model. The typical range for  $B_0$  in this model is  $[0, 1]$  and is related to  $\lambda_1$  by

$$B_0 = \frac{2\lambda_1^2 H_0^2}{c^2}. \quad (10)$$

We calculate  $E_G(k, z)$  for GR,  $f(R)$  gravity, and chameleon gravity using MGCAMB (Lewis et al. 2000; Hojjati et al. 2011), which we plot in Fig. 1. In GR,  $E_G$  is scale-independent. However, in  $f(R)$  gravity  $E_G$  decreases at small scales by  $\sim 10\%$ , with the decrease being more pronounced at higher redshifts and smaller scales. On the other hand, chameleon gravity shifts  $E_G$  to lower values with respect to GR. These results show that the ability to measure the scale-dependence of  $E_G$  will be advantageous for constraining MG models, particularly for  $f(R)$  gravity.

### 3. ESTIMATOR

Here we derive an estimator for  $E_G$  in terms of the galaxy-convergence cross-power spectrum  $C_\ell^{g\kappa}$ , the galaxy auto-power spectrum  $C_\ell^{gg}$ , and the RSD parameter  $\beta$ . The estimator is similar to the expression in Reyes et al. (2010) using the galaxy-galaxy lensing cross-power spectrum.

Starting with Eq. 1,  $E_G$  can be estimated in terms of power spectra as

$$\hat{E}_G(k, z) = \frac{c^2 \hat{P}_{\nabla^2(\psi-\phi)g}(k)}{3H_0^2(1+z)\hat{P}_{\theta g}(k)}, \quad (11)$$

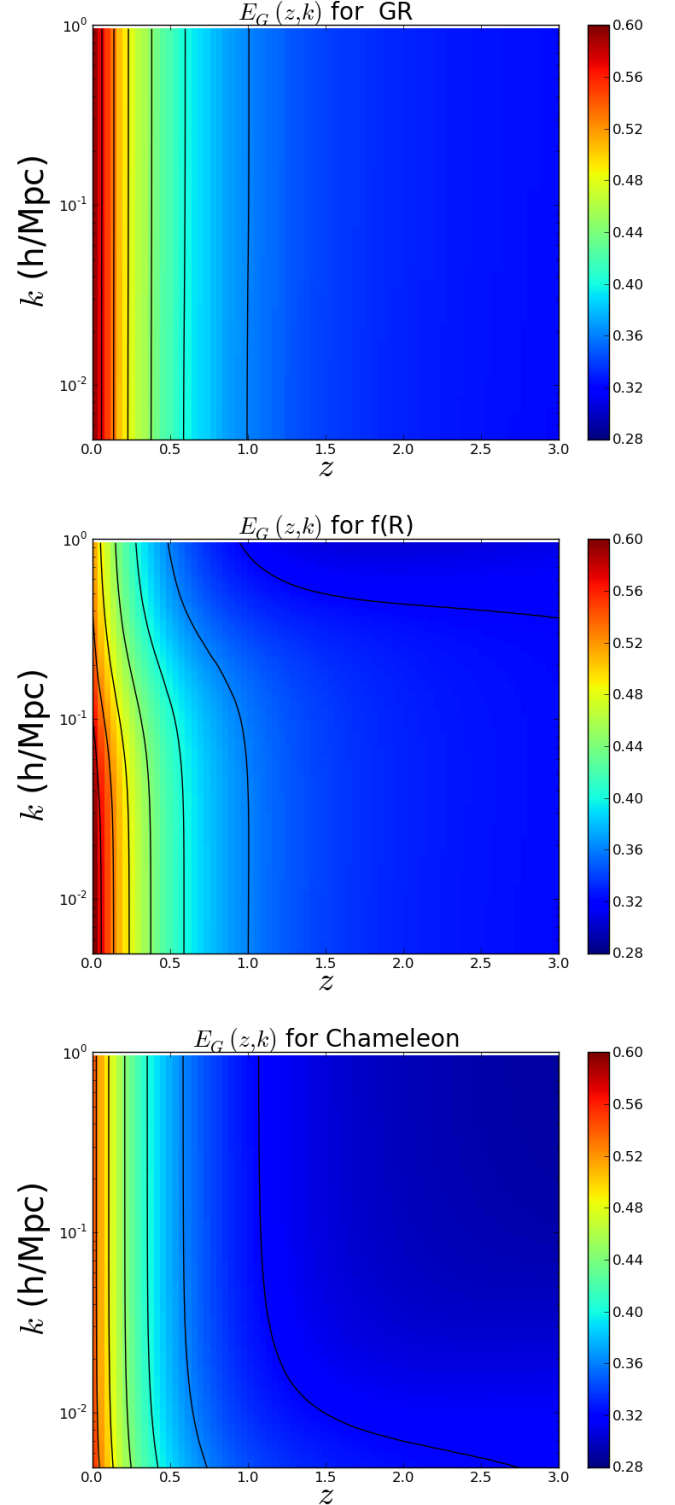


**Figure 1.**  $E_G$  as a function of redshift  $z$  and wavenumber  $k$  for GR (top),  $f(R)$  gravity ( $B_0 = 5.6 \times 10^{-5}$ ) (middle), and chameleon gravity ( $\beta_1 = 1.2$ ,  $B_0 = 0.4$ ,  $s = 4$ ) (bottom).  $E_G$  for  $f(R)$  gravity exhibits strong scale dependence, decreasing by  $\sim 10\%$  at small scales.

where  $P_{\nabla^2(\psi-\phi)g}$  is the galaxy- $\nabla^2(\psi-\phi)$  cross-power spectrum and  $P_{\theta g}$  is the galaxy-peculiar velocity cross-power spectrum. Projecting 3D power spectra into angular quantities, we can estimate  $E_G$  as

$$\hat{E}_G(\ell, \bar{z}) = \frac{c^2 \hat{C}_\ell^{\kappa g}}{3H_0^2 \hat{C}_\ell^{\theta g}}. \quad (12)$$

$C_\ell^{\kappa g}$  is the galaxy-convergence angular cross-power spectrum, given on small scales using the Limber approximation<sup>1</sup> by

$$C_\ell^{\kappa g} = \frac{1}{2} \int_{\chi_1}^{\chi_2} d\chi W(\chi) f_g(\chi) \chi^{-2} P_{\nabla^2(\psi-\phi)g} \left( \frac{\ell}{\chi}, z \right) \quad (13)$$

where  $f_g$  is the galaxy redshift distribution,  $\chi_1$  and  $\chi_2$  are the limits of the redshift distribution, and  $W(\chi) = \chi(1 - \chi/\chi_{\text{CMB}})$  is the CMB lensing kernel. In order to match the kernel in the galaxy-convergence power spectrum, we define  $C_\ell^{\theta g}$ , the velocity-galaxy angular cross-power spectrum, to be

$$C_\ell^{\theta g} = \frac{1}{2} \int_{\chi_1}^{\chi_2} d\chi W(\chi) f_g(\chi) \chi^{-2} (1+z) P_{\theta g} \left( \frac{\ell}{\chi}, z \right) \quad (14)$$

This cross-power spectrum is a construct used to measure  $E_G$  without multiplicative bias, and is not equivalent to the RSD angular power spectrum derived in Padmanabhan et al. (2007).

In our analysis, as in Reyes et al. (2010), we assume that the RSD parameter  $\beta$  will be measured separately, and we approximate the lensing kernel and  $\beta$  as constants over redshift within the integral, and we approximate  $f_g(\chi) \simeq f_g^2(\chi)/f_g(\bar{\chi})$  within the redshift range. This approximation works well when the galaxy redshift distribution is highly peaked, which is especially true when we use small redshift bins in forecasts for upcoming surveys. Also, we assume from linear theory  $\theta = f\delta$ . In that case, Eq. 14 can be written as

$$\begin{aligned} C_\ell^{\theta g} &\simeq \frac{W(\bar{\chi})(1+\bar{z})}{2f_g(\bar{\chi})} \int_{\chi_1}^{\chi_2} d\chi f_g^2(\chi) \chi^{-2} \beta(z) P_{gg} \left( \frac{\ell}{\chi}, z \right) \\ &\simeq \frac{W(\bar{\chi})\beta(\bar{z})(1+\bar{z})}{2f_g(\bar{\chi})} C_\ell^{gg}, \end{aligned} \quad (15)$$

where  $C_\ell^{gg}$  is the galaxy angular auto-power spectrum. Note that  $\beta$  could exhibit scale-dependence due to modified gravity through the growth rate. Thus,  $E_G$  in this case can be written as

$$\hat{E}_G(\ell, \bar{z}) = \frac{2c^2 \hat{C}_\ell^{\kappa g}}{3H_0^2 (1+\bar{z}) W(\bar{\chi}) \Delta\chi \beta(\bar{z}) \hat{C}_\ell^{gg}}, \quad (16)$$

and we can write the error of  $E_G$  in terms of the errors of  $\beta$  and  $C_\ell^{gg}$  as

$$\frac{\sigma^2[E_G(\ell, \bar{z})]}{E_G^2} = \left[ \left( \frac{\sigma(C_\ell^{\kappa g})}{C_\ell^{\kappa g}} \right)^2 + \left( \frac{\sigma(\beta)}{\beta} \right)^2 + \left( \frac{\sigma(C_\ell^{gg})}{C_\ell^{gg}} \right)^2 \right] \quad (17)$$

which is strictly true if  $\beta$  and  $C_\ell^{gg}$  are measured from separate surveys. This approximation does underestimate the error if  $\beta$  and  $C_\ell^{gg}$  are measured from the same

<sup>1</sup> Since we are mainly interested in small scales ( $\ell \gtrsim 100$ ), the Limber approximation is valid for most of the cases we consider (see Sec. 4.2)

survey. However, it should not be much of a concern for us. For current surveys and upcoming spectroscopic surveys, the error is mainly dominated by the CMB lensing, which is a measure independent of  $\beta$  and  $C_\ell^{\kappa g}$ . For example, switching between independent to dependent measures of  $\beta$  and  $C_\ell^{gg}$  for BOSS reduces the signal-to-noise ratio for  $E_G$  by 1%. For upcoming photometric surveys when the lensing error is competitive with the error in  $\beta$ , the error in the galaxy clustering due to shot noise should be small enough such that it can be neglected, making the  $\beta C_\ell^{gg}$  error independent of this concern. For example, switching between independent to dependent measures of  $\beta$  and  $C_\ell^{gg}$  for *Euclid* photometric survey with Adv. ACTPol reduces the signal-to-noise ratio for  $E_G$  by 5%. The uncertainty in  $C_\ell^{\kappa g}$  can be written as

$$\sigma^2(C_\ell^{\kappa g}) = \frac{(C_\ell^{\kappa\kappa})^2 + (C_\ell^{\kappa\kappa} + N_\ell^{\kappa\kappa})(C_\ell^{gg} + N_\ell^{gg})}{(2\ell + 1)f_{\text{sky}}}, \quad (18)$$

where  $C_\ell^{\kappa\kappa}$ , the convergence auto-power spectrum, is computed from CAMB (Lewis et al. 2000),  $N_\ell^{\kappa\kappa}$  is the noise in the convergence power spectrum computed using the formalism in Hu & Okamoto (2002), and  $N_\ell^{gg}$  is the shot noise.

A precise measurement of  $E_G$  will be slightly biased from the true value due to several reasons similar to those outlined in the Appendix of Reyes et al. (2010). For one, galaxy redshift distributions can exhibit a spread and skewness, causing the approximation in Eq. 15 to break down. However, we can characterize this deviation analytically as a function of angular scale. Also, in order to extend our measurement of  $E_G$  to small scales, we must correct for the scale-dependence of the bias due to clustering at nonlinear scales. We may also need to consider scale-dependent  $\beta$  due to nonlinear density and velocity perturbations, although velocity perturbations tend to stay linear at smaller scales than for density perturbations. In addition, constraints on modified gravity parameters will have to account for the scale dependence of  $\beta$  due to the growth rate. We expect these effects to be small and will neglect them in our forecasts.

#### 4. FORECASTS

In this section we will predict the ability of current and future surveys to measure  $E_G$  and differentiate between GR and MG models. In all our forecasts we will assume GR when calculating uncertainties. We describe the sensitivity of the measured  $E_G$  with the signal-to-noise ratio (SNR) of  $E_G$  marginalized over angular scale and redshift, given by

$$\text{SNR}^2(E_G) = \sum_{\ell, z_i} \frac{[E_G^{\text{GR}}(z_i)]^2}{\sigma^2[E_G(\ell, z_i)]}, \quad (19)$$

where  $z_i$  denotes redshift bins. We also calculate the  $\chi^2$  value between GR and MG models to determine if a particular  $E_G$  measurement could distinguish between GR and a given MG model. We write  $\chi^2$  as

$$\chi^2(E_G) = \sum_{\ell, z_i} \frac{[E_G^{\text{MG}}(\ell, z_i) - E_G^{\text{GR}}(z_i)]^2}{\sigma^2[E_G(\ell, z_i)]}, \quad (20)$$

where  $E_G^{\text{MG}}(\ell, z_i)$  is the  $E_G$  estimate for a given MG model, which is generally  $\ell$ -dependent. This  $\chi^2$  is related

**Table 1**

Properties of the various spectroscopic surveys considered in our analysis.

Survey	$z$	Area (deg <sup>2</sup> )	$N_{\text{gal}}$
BOSS CMASS	0.43–0.7	7900	704,000
BOSS LOWZ	0.15–0.43	6900	306,000
BOSS QSOs	2.1–3.5	10,200	175,000
DESI ELGs	0.6–1.7	14,000	$1.8 \times 10^7$
DESI LRGs	0.6–1.2	14,000	$4.1 \times 10^6$
DESI QSOs	0.6–1.9	14,000	$1.9 \times 10^6$
<i>Euclid</i>	0.5–2.0	20,000	$1.7 \times 10^7$
WFIRST	1.05–2.9	2000	$3.0 \times 10^7$

to the likelihood ratio between GR and modified gravity, assuming modified gravity is the true theory, and  $\chi^2 \gg 1$  means the two theories can be differentiated at high significance. Throughout the section we quote  $\chi_{\text{rms}} = \sqrt{\chi^2}$ . Note that for the following limits,  $f(R)$  gravity is set to its upper limit value  $B_0 = 5.6 \times 10^{-5}$ , and that chameleon gravity’s base set of parameters is  $B_0 = 0.4$ ,  $\beta_1 = 1.2$ , and  $s = 4$ , unless otherwise stated.

#### 4.1. Current Surveys

We begin with forecasts of  $E_G$  measurements from the publicly available *Planck* CMB lensing map (Planck Collaboration et al. 2014) and the CMASS and LOWZ spectroscopic galaxy samples from BOSS DR11 (Anderson et al. 2014), as well as the spectroscopic quasar (QSO) sample (Pâris et al. 2014) from DR11. We use the noise estimate given in the public *Planck* CMB lensing map. The total number of galaxies (or quasars) within each sample along with the survey area are listed in Table 1. For CMASS, we use the measurements of  $b\sigma_8$  and  $f\sigma_8$  from Samushia et al. (2014) to set  $b[\text{CMASS}] = 2.16$  and  $\sigma(\beta)/\beta \sim 10\%$  for the entire redshift range. The corresponding values for the LOWZ sample have not been measured model-independently for DR11, so we assume a 10% measurement of  $\beta$  for the entire redshift range and, as in Tojeiro et al. (2014), we assume  $b[\text{LOWZ}] = 1.85$ . We use Eq. 17 to calculate the  $E_G$  uncertainty for these samples. For the BOSS quasar sample, we use the BOSS DR9 bias measurements from White et al. (2012), assuming the average value  $b_{\text{QSO}} = 3.83$ . We also assume a 15%  $\beta$  measurement in each of two redshift bins for the BOSS quasars. This is a bit optimistic, considering there are systematic issues on linear scales with measuring RSD from BOSS quasars. However, we confirm that even a measurement error of 100% [ $\sigma(\beta)/\beta = 1$ ] only increases the errors on  $E_G$  by 5%.

We plot the signal-to-noise ratio (SNR) for  $10 < \ell < 1000$  for the CMASS, LOWZ, and quasar samples in Fig. 2. The peaks of all three plots vary due to the redshift of each sample. We find that most of the signal for  $E_G$  comes from linear to quasi-linear scales. We set the maximum wavenumber within quasi-linear scales to  $k_{\text{NL}}$ , where  $\Delta(k_{\text{NL}}, z) = k_{\text{NL}}^3 P(k_{\text{NL}}, z)/(2\pi^2) = 1$ . We find  $k_{\text{NL}}[\text{LOWZ}, \text{CMASS}] = [0.354, 0.466] \text{ h/Mpc}$ . For the following forecasts, we limit the angular scales used to  $\ell > 100$  to avoid large-scale systematic effects. In Fig. 2 we also show how the SNR increases with  $\ell_{\text{max}}$  for CMASS and LOWZ. We see that most of the sensitivity is obtained by  $\ell \sim 500$  for CMASS and  $\ell \sim 300$  for LOWZ. We set these as our limits in  $\ell$  for CMASS and LOWZ, while for quasars we will use all scales  $\ell < 1000$ .

We also consider how our forecasts for  $E_G$  are affected if we restrict the scales used to measure  $E_G$  to only linear scales for CMASS and LOWZ. Note we define linear scales  $k < k_{\text{lin}}$  as those for which the matter power spectrum  $P(k)$  computed from N-body simulations differs from the linear  $P(k)$  by less than a few percent. We determine which scales are linear using the linear and N-body  $P(k)$  predictions from Fig. 2 of Vlah et al. (2014). We find that the purely linear scales for CMASS and LOWZ are limited to  $k \lesssim 0.1 \text{ h/Mpc}$ , which is significantly less than  $k_{\text{NL}}$  determined above for these surveys. As can be seen in Fig. 2, the surveys each lose about half their signal to noise if the measurements are restricted to linear scales.<sup>2</sup> Note that as the redshift of the survey increases, the more scales are linear. However,  $E_G$  estimates for modified gravity, particularly for  $f(R)$  gravity, tend to differ from GR mainly at low redshifts. Thus, differentiating MG models from GR requires measuring  $E_G$  at quasi-linear scales.

Next we forecast constraints on  $E_G$  from BOSS surveys cross-correlated with the *Planck* CMB lensing map. We find promising results, listed in Table 2. Specifically, we predict SNRs of 9.3, 5.2, and 6.8 for the CMASS, LOWZ, and QSO surveys, respectively. We translate these into  $E_G$  values in Fig. 3. We see that our LOWZ measurement would be comparable to that from Reyes et al. (2010), although this may be somewhat optimistic considering LOWZ may exhibit unforeseen systematics. However, combining all three measurements would give a SNR of 13, or an 8% measurement. This assumes we can measure RSD from quasars, which is very optimistic considering systematic errors that exist in quasars at large scales (Pullen & Hirata 2013). We also consider our fiducial model of  $f(R)$  gravity corresponding to the upper limit on the BZ parameter  $B_0$ . We see that the  $f(R)$  prediction differs from GR only at lower redshifts, greatly suppressing the utility of the quasar measurement and slightly increasing the utility of the LOWZ measurement.  $\chi_{\text{rms}} = \sqrt{\chi^2}$  for CMASS and LOWZ are both less than unity, implying that these surveys are not able to significantly tighten constraints on  $B_0$ . The sensitivity to chameleon gravity is only slightly better, in that CMASS, LOWZ, and BOSS QSOs together could differentiate models with very high (or low) values of  $\beta_1$  from GR due to the rapid evolution of  $E_G$  with  $\beta_1$ .

#### 4.2. Upcoming Spectroscopic Surveys

We now consider upcoming spectroscopic surveys. We consider two cases for the CMB lensing map, including (1) the full *Planck* CMB lensing map and (2) the Advanced ACTPol<sup>3</sup> CMB lensing map. In both cases, we assume the CMB lensing maps will be estimated using the temperature map and both  $E$  and  $B$  polarization maps, and we assume the  $B$  map only contains noise. We predict the noise in the *Planck* lensing map assuming the detector sensitivity and beam sizes listed in the *Planck* Bluebook (The Planck Collaboration 2006). Advanced ACTPol will survey 20,000 deg<sup>2</sup>, and its increased temperature and polarization sensitivity will create a CMB lensing map that is an order of magnitude more sensitive

<sup>2</sup>  $\ell_{\text{lin}}[\text{LOWZ}] < 100$ , so we set  $\ell_{\text{min}}[\text{LOWZ}] = 50$  when considering the total signal.

<sup>3</sup> private communication with Advanced ACTPol team

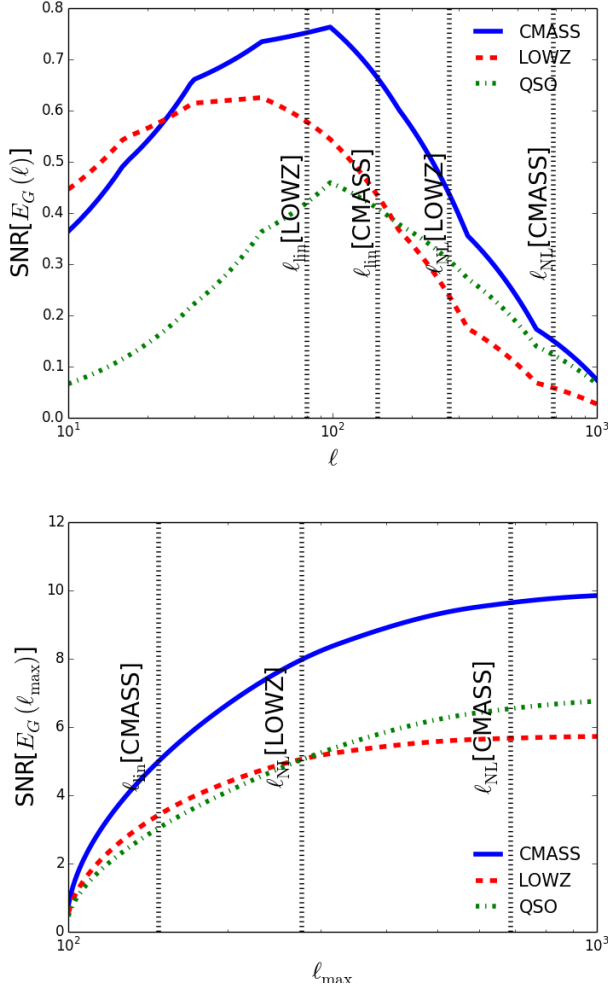


**Figure 2.** (Top): The SNR of  $E_G$  as a function of  $\ell$  for the *Planck* CMB lensing map cross-correlated with various BOSS DR11 surveys. We also mark with vertical lines where the angular modes correspond to nonlinear scales. We see that most of the sensitivity will come from linear scales, although our chosen cuts in  $\ell$  listed in the text will lose some sensitivity. (Bottom): The relation of the SNR of  $E_G$  with an increasing  $\ell_{\max}$  for the BOSS DR11 samples with the *Planck* CMB lensing map. We see that most of the sensitivity is gained using  $\ell_{\max} \sim 300$  (500) for LOWZ (CMASS), while the sensitivity for the QSO sample is still increasing at  $\ell_{\max} = 1000$ .

than *Planck*. The specifications we use for Adv. ACT-Pol are listed in Table 3. For spectroscopic surveys, we consider the DESI emission line galaxy (ELG), luminous red galaxy (LRG), and quasar surveys, as well as the *Euclid* H $\alpha$  survey and the WFIRST H $\alpha$  and OIII combined survey. The properties of the surveys are listed in Table 1. For DESI, we assume the same values as in the DESI Conceptual Design Report<sup>4</sup>:  $b_{\text{LRG}}D(z) = 1.7$ ,  $b_{\text{ELG}}D(z) = 0.84$ ,  $b_{\text{QSO}}D(z) = 1.2$ , where  $D(z)$  is the growth factor. We also assume a 4% error in  $\beta$  within  $\Delta z = 0.1$  bins. Note that Adv. ACTPol’s survey area overlaps with only  $\sim 75\%$  of DESI’s area; we take this into account in our DESI forecasts. For *Euclid* and WFIRST ELGs, we assume  $b(z) = 0.9 + 0.4z$ , a fit (Takada et al. 2014) to semi-analytic models (Orsi et al. 2010) that com-

<sup>4</sup> <http://desi.lbl.gov/cdr/>

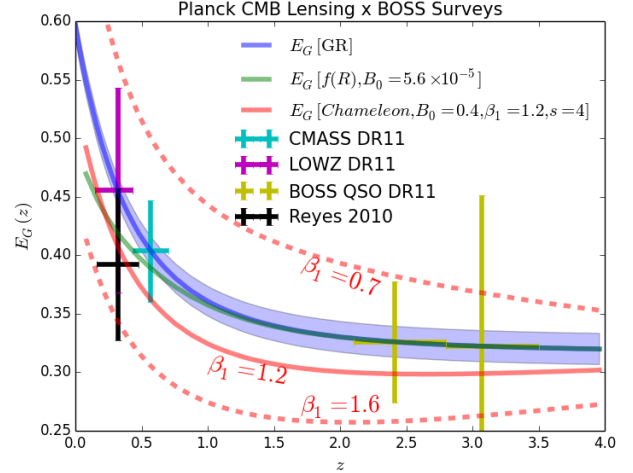


**Figure 3.**  $E_G$  forecasts for BOSS galaxy surveys cross-correlated with the current *Planck* CMB lensing map, in comparison with the latest measurement of  $E_G$  using galaxy-galaxy lensing (Reyes et al. 2010). Note that we do not translate their  $E_G$  measurement from the WMAP3 cosmology (Spergel et al. 2007) to the cosmology we assume. The band around the GR prediction corresponds to the likelihood function of  $E_G$  based on *Planck* and BOSS constraints on cosmological parameters. The  $E_G$  predictions for  $f(R)$  gravity and chameleon gravity are averaged over the wavenumber range at every redshift corresponding to  $100 < \ell < 500$ , the range used for CMASS. The dashed lines show chameleon gravity predictions for higher and lower values of  $\beta_1$ . These surveys are not sensitive enough to tighten constraints on  $f(R)$  gravity set by current measurements.

pares well with data. We determine the redshift distribution of *Euclid* H $\alpha$  galaxies using the H $\alpha$  luminosity function from Colbert et al. (2013) and assume a flux limit of  $4 \times 10^{-16}$ . This flux limit is in the middle of the range being considered, so the following *Euclid* forecasts can change accordingly. We also assume a 3% error in  $\beta$  within  $\Delta z = 0.1$  bins for *Euclid* and WFIRST (Amendola et al. 2013). For all subsequent forecasts, we assume  $E_G$  measurements over angular scales  $100 \leq \ell \leq 500$ .

The forecasts are listed in Table 2, but here we list some highlights. Figs. 4 and 5 show that DESI and *Euclid* combined with *Planck* can each measure  $E_G$  almost at the 2% level, unlike WFIRST which is limited by its small survey area. This should allow DESI and *Euclid* combined with *Planck* to produce constraints of some models, and  $\beta_1$  constraints should get tighter than those from BOSS. For Adv. ACTPol, DESI should reach a 1% measurement of  $E_G$ , allowing it to differentiate GR and chameleon gravity with  $\beta_1 > 1.1$  at the  $5\sigma$  level. DESI produces tighter constraints than *Euclid* due to its higher number density at low redshifts. Note that we use a moderate number of redshift slices for each survey, as seen in Figs. 4 and 5. The redshift accuracy of these spectroscopic surveys would allow us to use much smaller redshift bins in an attempt to decrease errors in  $E_G$ . This does not work, however, because each of these surveys are shot-noise dominated on the scales where the  $E_G$  signal dominates, increasing the errors in the galaxy-



CMB lensing cross-correlation.<sup>5</sup> We also considered more pessimistic errors in  $\beta$ , finding that increasing the error in  $\beta$  by a factor of 3 did not noticeably increase  $E_G$  errors from *Planck*, while it increased  $E_G$  errors from Adv. ACTPol by less than 2%.

#### 4.3. Upcoming Photometric Surveys

In this section we consider measuring  $E_G$  from upcoming photometric galaxy surveys. These surveys, which measure less precise redshifts than spectroscopic surveys, are tailored for measuring weak lensing and not RSD. However, the errors in  $E_G$  are dominated by the CMB lensing at lower redshifts where the  $E_G$  signal is highest, meaning that reducing shot noise in the lensing-galaxy cross-correlation through attaining higher number densities is more important than having precise redshifts. Also, upcoming photometric surveys plan to approach redshift precisions of  $\sigma_z/(1+z) \sim 0.05$ . Recent work has shown that upcoming photometric surveys could measure RSD (Ross et al. 2011; Crocce et al. 2011; Asorey et al. 2014). This may cause photometric surveys to produce competitive  $E_G$  measurements. It should be noted that Adv. ACTPol gets close to the lensing noise limit where errors in RSD could begin to matter. An  $E_G$  measurement from a future CMB experiment that surpasses Adv. ACTPol may reach the limit such that RSD errors may begin to dominate. Also, the photometric redshift errors and systematic errors within photometric surveys will make measuring RSD with photometric surveys more difficult than with spectroscopic surveys (Ho et al. 2012).

We will construct forecasts for photometric surveys of DES, LSST, and *Euclid*. The properties of these surveys are listed in Table 4. For DES and LSST, we model the normalized redshift distribution in the same manner as Font-Ribera et al. (2014) as

$$f_g(z) = \frac{\eta}{\Gamma\left(\frac{\alpha+1}{\eta}\right)} \left(\frac{z}{z_0}\right)^\alpha \exp^{-(z/z_0)^\eta}, \quad (21)$$

where  $\alpha = 1.25$  (2.0),  $\eta = 2.29$  (1.0), and  $z_0 = 0.88$  (0.3) for DES (LSST). For *Euclid* we use estimates of the redshift distribution based on the CANDELS GOODS-S catalog (Guo et al. 2013; Hsu et al. 2014). For all three surveys we assume  $b(z) = 0.9 + 0.4z$  (Takada et al. 2014; Orsi et al. 2010), as in the spectroscopic case. For RSD, we assume a 17% error in  $\beta$  over  $\Delta z = 0.1(1+z)$  bins for DES (Ross et al. 2011). Since *Euclid* and LSST will cover about 4 times the volume of DES, we expect the errors on  $\beta$  to decrease by a factor of 2.

We find that photometric surveys can discriminate between gravity models more effectively than spectroscopic surveys, as can be seen in Fig. 6 and Table 2. DES, with its higher number density, has constraining power comparable to DESI and *Euclid* with their larger survey areas. LSST and photometric *Euclid* combined with *Planck* approach 1% measurements, while substituting *Planck* for Adv. ACTPol exceeds that level. In Fig. 7, we display constraints on  $E_G$  in individual  $k$ -bins at

<sup>5</sup> Using the formalism in LoVerde & Afshordi (2008), the Limber approximation breaks down slightly for *Euclid* with Adv. ACTPol at some of the larger redshifts, where  $\chi/\Delta\chi \gtrsim 100$ . This should not affect the results significantly.

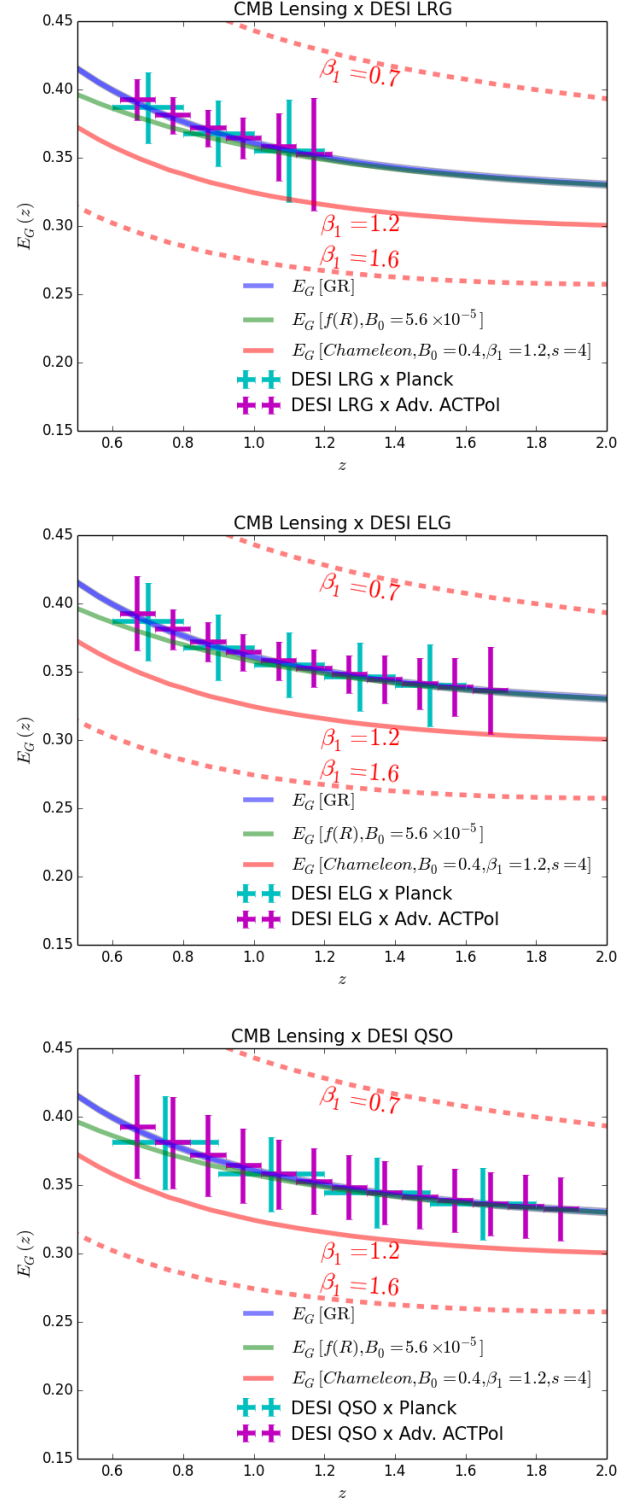


**Figure 4.**  $E_G$  forecasts for DESI galaxy surveys cross-correlated with the final *Planck* CMB lensing map and with the Advanced ACTPol lensing map. The points for Adv. ACTPol are shifted rightward by 0.02 for clarity. The  $E_G$  predictions for  $f(R)$  and chameleon gravity are averaged over the wavenumber range at every redshift corresponding to  $100 < \ell < 500$ . The dashed lines show chameleon gravity predictions for higher and lower values of  $\beta_1$ .

**Table 2**

Forecasts of the signal-to-noise ratio (SNR) and  $\chi_{\text{rms}} = \sqrt{\chi^2}$  between GR and  $f(R)$  or chameleon gravity for  $E_G$  measurements from various current and upcoming surveys. For  $f(R)$  gravity, we assume  $B_0 = 5.65 \times 10^{-5}$ . For chameleon gravity, the first column assumes  $B_0 = 3.2 \times 10^{-4}$  with  $\beta_1$  and  $s$  set to the base model, and the second column assumes  $\beta_1 = 1.1$  with  $B_0$  and  $s$  set to the base model (see the beginning of Sec. 4).

Survey (Galaxy $\times$ CMB lensing)	$z$	SNR	$\chi_{\text{rms}}[f(R)]$	$\chi_{\text{rms}}[\text{Cham}, B_0]$	$\chi_{\text{rms}}[\text{Cham}, \beta_1]$
BOSS CMASS $\times$ <i>Planck</i> (current)	0.43–0.7	9.3	0.40	0.53	0.52
BOSS LOWZ $\times$ <i>Planck</i> (current)	0.15–0.43	5.2	0.42	0.42	0.30
BOSS QSOs $\times$ <i>Planck</i> (current)	2.1–3.5	6.8	0.051	0.042	0.26
BOSS (CMASS+LOWZ+QSOs) $\times$ <i>Planck</i> (current)	–	13	0.58	0.68	0.65
DESI ELGs $\times$ <i>Planck</i> (full)	0.6–1.7	31	0.51	0.84	1.5
DESI LRGs $\times$ <i>Planck</i> (full)	0.6–1.2	23	0.55	0.83	1.1
DESI QSOs $\times$ <i>Planck</i> (full)	0.6–1.9	25	0.29	0.52	1.2
DESI (ELG+LRG+QSO) $\times$ <i>Planck</i> (full)	–	46	0.80	1.3	2.2
DESI ELGs $\times$ Adv. ACTPol	0.6–1.7	73	1.4	2.3	3.6
DESI LRGs $\times$ Adv. ACTPol	0.6–1.2	56	1.8	2.5	2.9
DESI QSOs $\times$ Adv. ACTPol	0.6–1.9	50	0.66	1.1	2.4
DESI (ELG+LRG+QSO) $\times$ Adv. ACTPol	–	105	2.4	3.6	5.2
<i>Euclid</i> (spectro) $\times$ <i>Planck</i> (full)	0.5–2.0	41	0.96	1.4	2.1
<i>Euclid</i> (spectro) $\times$ Adv. ACTPol	0.5–2.0	83	2.4	3.2	4.1
WFIRST $\times$ <i>Planck</i> (full)	1.05–2.9	20	0.12	0.21	0.91
WFIRST $\times$ Adv. ACTPol	1.05–2.9	44	0.28	0.55	2.0
DES $\times$ <i>Planck</i> (full)	0.0–2.0	35	1.2	1.3	1.7
DES $\times$ Adv. ACTPol	0.0–2.0	78	3.0	3.3	3.9
LSST $\times$ <i>Planck</i> (full)	0.0–2.5	84	5.1	5.2	6.0
LSST $\times$ Adv. ACTPol	0.0–2.5	189	15	15	16
<i>Euclid</i> (photo) $\times$ <i>Planck</i> (full)	0.0–3.7	90	4.9	5.1	5.9
<i>Euclid</i> (photo) $\times$ Adv. ACTPol	0.0–3.7	205	15	15	16

**Table 3**

Properties of the Advanced ACTPol CMB survey. Note that the area of the survey is 20,000 deg<sup>2</sup> and we assume  $\Delta_P = \Delta_T \sqrt{2}$ .

Center Freq.	$\Delta_T$ ( $\mu\text{K-arcmin}$ ) <sup>a</sup>	$\theta_{\text{res}}$ (arcmin)
90 GHz	7.8	2.2
150 GHz	6.9	1.3
230 GHz	25	0.9

<sup>a</sup>per resolved pixel

**Table 4**

Properties of various galaxy photometric surveys included in our analysis.

Survey	$z$	Area (deg <sup>2</sup> )	$N_{\text{gal}}$	$\sigma_z/(1+z)$
DES	0.0–2.0	5000	$2.16 \times 10^8$	0.07
LSST	0.0–2.5	20,000	$3.6 \times 10^9$	0.05
<i>Euclid</i>	0.0–3.7	20,000	$1.86 \times 10^9$	0.05

$z = 1 \pm 0.05$  from LSST with both CMB surveys, finding that at this redshift the constraining power between gravity models mainly appears at smaller scales. These two photometric surveys combined with Adv. ACTPol could differentiate  $f(R)$  gravity and GR at the  $13\sigma$  level for  $B_0 > 10^{-7}$ , severely testing  $f(R)$  as a viable theory. These surveys also would place significant tests on chameleon gravity, although the value of  $\chi^2$  decreases when smaller values of  $B_0$  are assumed. Also, catastrophically increasing the errors in  $\beta$  by a factor of 3 in DES increases the errors in  $E_G$  using *Planck* by only 5%. Similar increases also apply to *Euclid* and WFIRST. For Adv. ACTPol,  $E_G$  is more sensitive to this effect, in that increasing  $\beta$  errors by a factor of 3 increases  $E_G$  errors by 20%. This suggests that in this regime, RSD errors must remain low to take advantage of the power of photometric surveys to measure  $E_G$ , on the order of 10% for *Euclid* or LSST.

## 5. CONCLUSIONS

In this work we consider CMB lensing as a probe of  $E_G$ , a statistic that differentiates between gravity models on cosmological scales. We derive  $E_G$  for the general MG parametrization described by  $\mu(k, z)$  and  $\gamma(k, z)$ , as well as for the specific MG models of  $f(R)$  gravity and chameleon gravity. We show that generally,  $E_G$  for these models are scale-dependent, causing the scale-dependent  $E_G$  to be useful for differentiating between MG models and GR.

We produce forecasts for current surveys, showing that BOSS spectroscopic galaxies and quasars combined with *Planck* CMB lensing each measure  $E_G$  at the 8% level. Our results suggest that CMB lensing contributes most of the error, and that measuring  $E_G$  on quasi-linear scales is required to produce significant constraints.

For upcoming surveys, we find that upcoming photometric surveys will outperform spectroscopic surveys due to their higher number densities, even at the expense of having less precise redshifts. Specifically, LSST and photometric *Euclid* should produce errors on  $E_G$  less than 1%, and place very tight constraints on  $f(R)$  and chameleon gravity, assuming these surveys can measure RSD with a precision of around 10%. However, these measurements will be limited by how well these photometric surveys can identify and remove systematic errors. Also, since it is necessary to use  $E_G$  from quasi-linear scales, measuring RSD effects at these scales will be challenging. Finally, it is possible that more precise estimates of  $E_G$  and more precise measurements of cosmological parameters may change the underlying  $E_G$  errors slightly. However, CMB lensing has the potential to probe  $E_G$  with very high sensitivities without the astrophysical contaminants of galaxy-galaxy lensing, and reveal the nature of gravity.

We thank O. Doré and D. Hanson for helpful comments



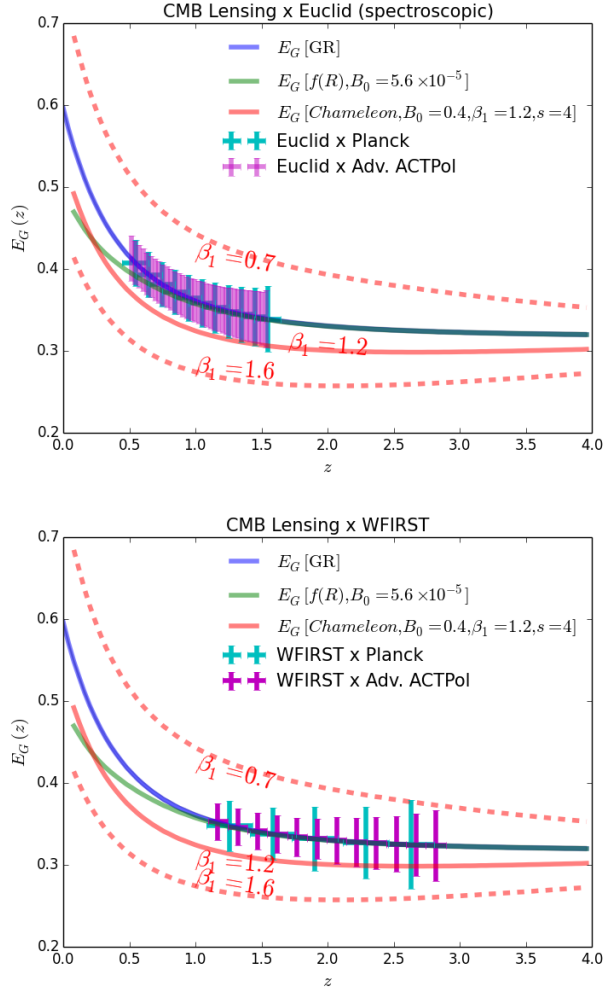


**Figure 5.**  $E_G$  forecasts for Euclid and WFIRST galaxy surveys cross-correlated with the final *Planck* CMB lensing map and with the Advanced ACTPol lensing map. The points for WFIRST and Adv. ACTPol are shifted rightward by 0.02 for clarity. Note the *Euclid*-Adv. ACTPol forecasts contain 50 bins in redshift.

on CMB lensing. We also thank D. Spergel for information on the specifications for Advanced ACTPol, as well as C. Hirata for redshift information for the *Euclid* photometric survey. AP was supported by a McWilliams Fellowship of the Bruce and Astrid McWilliams Center for Cosmology. SA and SH are supported by NASA grant 12-EUCLID11-0004 for this work. SH is also supported by DOE and NSF.

## REFERENCES

- Amendola, L., Appleby, S., Bacon, D., et al. 2013, *Living Reviews in Relativity*, 16, 6
- Anderson, L., Aubourg, É., Bailey, S., et al. 2014, *MNRAS*, 441, 24
- Asorey, J., Crocce, M., & Gaztañaga, E. 2014, *MNRAS*, 445, 2825
- Bel, J., Brax, P., Marinoni, C., & Valageas, P. 2014, *ArXiv e-prints*
- Bennett, C. L., Larson, D., Weiland, J. L., et al. 2013, *ApJS*, 208, 20
- Bertschinger, E., & Zukin, P. 2008, *Phys. Rev. D*, 78, 024015
- Blanchard, A., & Schneider, J. 1987, *A&A*, 184, 1
- Carroll, S. M., Duvvuri, V., Trodden, M., & Turner, M. S. 2004, *Phys. Rev. D*, 70, 043528

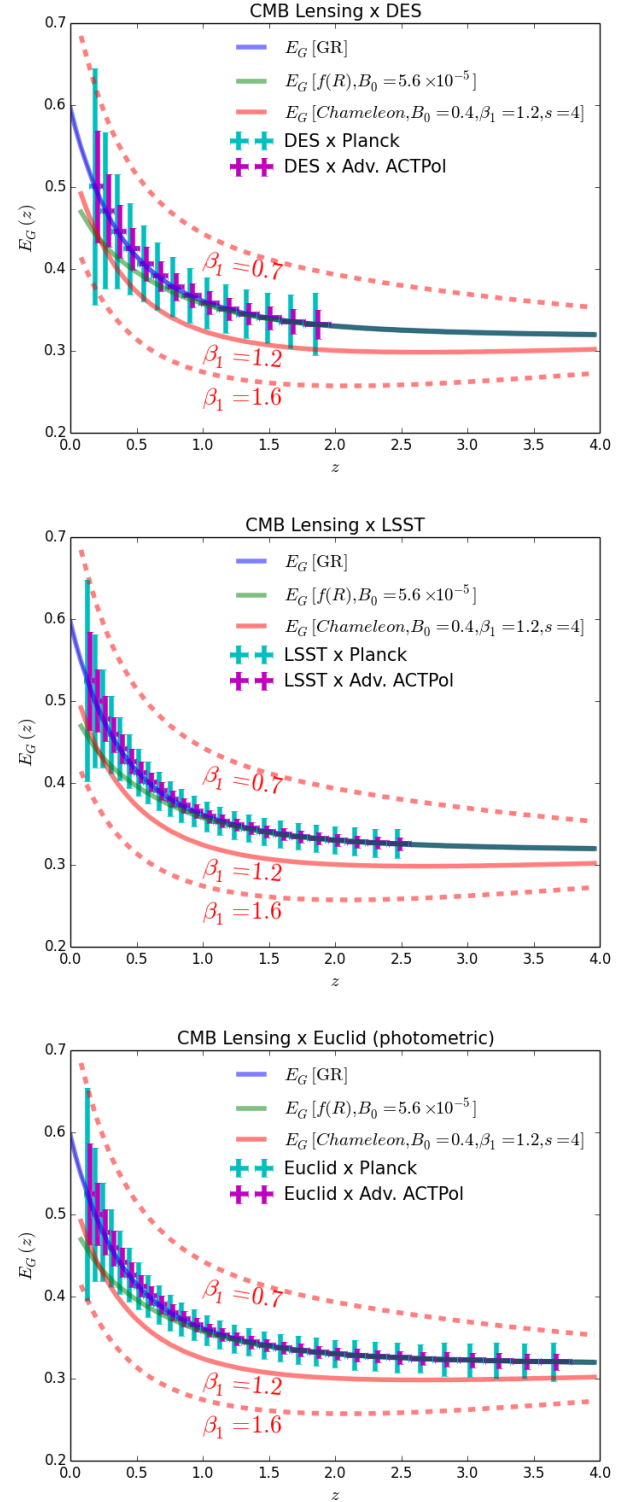


**Figure 6.**  $E_G$  forecasts for DES, LSST, and Euclid photometric galaxy surveys cross-correlated with the final *Planck* CMB lensing map and with the Advanced ACTPol lensing map. The points for Adv. ACTPol are shifted rightward by 0.02 for clarity. Note that the forecasts involving Adv. ACTPol require a precision in the RSD parameter  $\beta$  of 10%, which may need to be obtained from a spectroscopic survey.

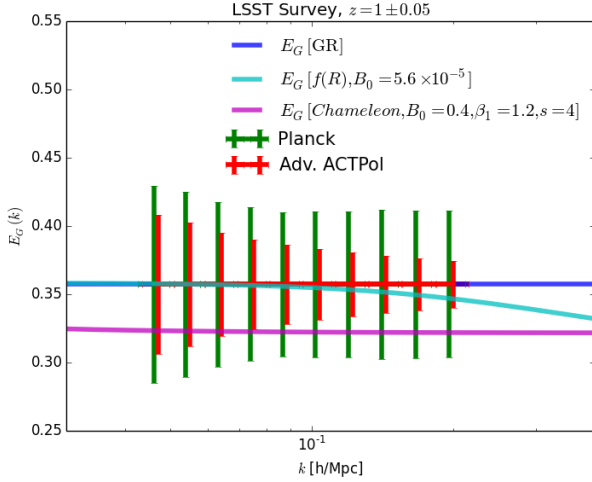


**Figure 7.**  $E_G(k)$  forecasts for the LSST photometric galaxy survey in the redshift bin  $z = 1 \pm 0.05$  cross-correlated with the final *Planck* CMB lensing map and with the Advanced ACTPol lensing map. The points for Adv. ACTPol are shifted rightward by 2% for clarity. We also plot  $E_G$  predictions for  $f(R)$  gravity and chameleon gravity.

Colbert, J. W., Teplitz, H., Atek, H., et al. 2013, *ApJ*, 779, 34  
 Cole, S., & Efstathiou, G. 1989, *MNRAS*, 239, 195  
 Crocce, M., Gaztañaga, E., Cabré, A., Carnero, A., & Sánchez, E. 2011, *MNRAS*, 417, 2577  
 Dawson, K. S., Schlegel, D. J., Ahn, C. P., et al. 2013, *AJ*, 145, 10  
 Dvali, G., Gabadadze, G., & Porrati, M. 2000, *Physics Letters B*, 485, 208  
 Eisenstein, D. J., Annis, J., Gunn, J. E., et al. 2001, *AJ*, 122, 2267  
 Eisenstein, D. J., Weinberg, D. H., Agol, E., et al. 2011, *AJ*, 142, 72  
 Font-Ribera, A., McDonald, P., Mostek, N., et al. 2014, *JCAP*, 5, 23  
 Guo, Y., Ferguson, H. C., Gialvalisco, M., et al. 2013, *ApJS*, 207, 24  
 Hirata, C. M., Ho, S., Padmanabhan, N., Seljak, U., & Bahcall, N. A. 2008, *Phys. Rev. D*, 78, 043520  
 Hirata, C. M., Padmanabhan, N., Seljak, U., Schlegel, D., & Brinkmann, J. 2004, *Phys. Rev. D*, 70, 103501  
 Ho, S., Cuesta, A., Seo, H.-J., et al. 2012, *ApJ*, 761, 14  
 Hojjati, A., Pogosian, L., & Zhao, G.-B. 2011, *JCAP*, 8, 5  
 Hsu, L.-T., Salvato, M., Nandra, K., et al. 2014, *ApJ*, 796, 60  
 Hu, W., & Okamoto, T. 2002, *ApJ*, 574, 566  
 Khoury, J., & Weltman, A. 2004, *Physical Review Letters*, 93, 171104

Laureijs, R., Amiaux, J., Arduini, S., et al. 2011, *ArXiv e-prints*  
 Levi, M., Bebek, C., Beers, T., et al. 2013, *ArXiv e-prints*  
 Lewis, A., Challinor, A., & Lasenby, A. 2000, *ApJ*, 538, 473  
 Linder, E. V. 1988, *A&A*, 206, 199  
 LoVerde, M., & Afshordi, N. 2008, *Phys. Rev. D*, 78, 123506  
 LSST Science Collaboration, Abell, P. A., Allison, J., et al. 2009, *ArXiv e-prints*  
 Orsi, A., Baugh, C. M., Lacey, C. G., et al. 2010, *MNRAS*, 405, 1006  
 Padmanabhan, N., Schlegel, D. J., Seljak, U., et al. 2007, *MNRAS*, 378, 852  
 Pâris, I., Petitjean, P., Aubourg, É., et al. 2014, *A&A*, 563, A54  
 Peebles, P. J., & Ratra, B. 2003, *Reviews of Modern Physics*, 75, 559  
 Perlmutter, S., Aldering, G., Goldhaber, G., et al. 1999, *ApJ*, 517, 565  
 Planck Collaboration, Ade, P. A. R., Aghanim, N., et al. 2013, *ArXiv e-prints*  
 —. 2014, *A&A*, 571, A17  
 Pullen, A. R., & Hirata, C. M. 2013, *PASP*, 125, 705  
 Reyes, R., Mandelbaum, R., Seljak, U., et al. 2010, *Nature*, 464, 256  
 Riess, A. G., Filippenko, A. V., Challis, P., et al. 1998, *AJ*, 116, 1009  
 Ross, A. J., Percival, W. J., Crocce, M., Cabré, A., & Gaztañaga, E. 2011, *MNRAS*, 415, 2193  
 Samushia, L., Reid, B. A., White, M., et al. 2014, *MNRAS*, 439, 3504  
 Smith, K. M., Zahn, O., & Doré, O. 2007, *Phys. Rev. D*, 76, 043510  
 Song, Y.-S., Hu, W., & Sawicki, I. 2007, *Phys. Rev. D*, 75, 044004  
 Spergel, D., Gehrels, N., Breckinridge, J., et al. 2013, *ArXiv e-prints*  
 Spergel, D. N., Bean, R., Doré, O., et al. 2007, *ApJS*, 170, 377  
 Takada, M., Ellis, R. S., Chiba, M., et al. 2014, *PASJ*, 66, 1  
 The Dark Energy Survey Collaboration. 2005, *ArXiv Astrophysics e-prints*  
 The Planck Collaboration. 2006, *ArXiv Astrophysics e-prints*  
 Tojeiro, R., Ross, A. J., Burden, A., et al. 2014, *MNRAS*, 440, 2222  
 Tsujikawa, S. 2007, *Phys. Rev. D*, 76, 023514  
 Vlah, Z., Seljak, U., & Baldauf, T. 2014, *ArXiv e-prints*  
 White, M., Myers, A. D., Ross, N. P., et al. 2012, *MNRAS*, 424, 933  
 Xu, L. 2014, *ArXiv e-prints*  
 York, D. G., Adelman, J., Anderson, Jr., J. E., et al. 2000, *AJ*, 120, 1579  
 Zhang, P., Liguori, M., Bean, R., & Dodelson, S. 2007, *Physical Review Letters*, 99, 141302